DUJASE Vol. 5(1 & 2) 1-8, 2020 (January & July)

Analysis of 2D Discrete Wavelet Transform Based Signal Denoising Technique in Brillouin Optical Time Domain Analysis Sensors

Abul Kalam Azad

Department of Electrical and Electronic Engineering, University of Dhaka, Dhaka-1000, Bangladesh

**E-mail: azad@du.ac.bd*

Received on 16 May 2020, Accepted for publication on 10 September 2020

ABSTRACT

In this paper, the use of 2D discrete wavelet transform (DWT) based wavelet denoising technique (WDT) is demonstrated experimentally to improve the signal-to-noise ratio (SNR) of the measured Brillouin gain spectra (BGSs) obtained along a 38. 2 km long fiber using Brillouin optical time domain analysis (BOTDA) sensor. The curve fitting method (CFM) was then applied to extract the distributions of Brillouin frequency shift (BFS) from the denoised BGSs. The performance of WDT-based CFM is evaluated in detail for the measured BGSs acquired with different frequency steps and different numbers of trace averaging. The variation of sensor spatial resolution with different decomposition levels adopted in WDT was also analyzed. The results showed that WDT can enhance the SNR of measured BGSs significantly. As a result, WDT-based CFM can improve the uncertainty in BFS extraction up to ~56% without sacrificing the spatial resolution as well as signal processing speed as compared to CFM without WDT. However, the measurement uncertainty can be improved further with a little sacrifice of spatial resolution. Moreover, under a given measurement uncertainty and spatial resolution, the WDT-based CFM can significantly reduce the acquisition time of BGSs by effectively adopting 5 times larger frequency step or 87. 50% less number of trace averaging to make BOTDA sensors suitable for faster operation.

Keywords: Distributed fiber optic sensors, Stimulated Brillouin scattering, Discrete wavelet transform, Least-square curve fitting, Lorentzian profile.

1. Introduction

Stimulated Brillouin scattering based Brillouin optical time domain analysis (BOTDA) sensors have been widely used in the past few decades for the distributed monitoring of strain and temperature along an optical fiber of several tens of kilometres with high accuracy and good spatial resolution [1 - 4]. In Brillouin gain configuration of such systems, two counter-propagating light waves (i. e. , pump and probe) induce an acoustic wave which scatters the pump wave through the process of electrostriction [5]. As a result, the power from the high frequency pump wave is transferred to amplify the low frequency probe wave. The power gained by the probe wave is characterized by the local Brillouin gain spectrum (BGS). The local BGS experiences maximum gain if the pump-probe frequency difference and the local Brillouin frequency shift (BFS) of the fiber under test (FUT) are exactly the same. In BOTDA sensor, the BFS along the FUT varies linearly with local strain or temperature. This linear relationship is utilized to extract distributed strain or temperature along the FUT.

The accurate extraction of BFS distributions in BOTDA sensors depends mainly on the SNR of the BGSs and BOTDA trace averaging is usually used to enhance the SNR [6, 7]. However, sufficient improvement of such SNR can only be achieved if thousands of BOTDA traces are acquired during experiment and all of these traces are then averaged to obtain a single trace. In such case, the acquisition of BGSs during experiment becomes time-consuming, particularly for a longer FUT. For the fast acquisition of BGSs, several alternative BOTDA schemes assisted by Raman amplification [8 - 10], pulse coding techniques [11 - 13] and combination of these [2, 14] have been studied recently to enhance such SNR. However, these alternative BOTDA schemes either require the modifications of hardware in the basic BOTDA setup or combine multiple techniques with basic BOTDA setup to build complex systems. On the other hand, the processing of signal using non-local means [15, 16] and wavelet transform [15 - 17] have also been studied in recent years for denoising the BGSs acquired from BOTDA sensors.

In particular, studies reported in [15 - 17] apply wavelet denoising technique to enhance the SNR of the BGSs and hence, uncertainty in BFS extraction by several orders of magnitude. Such technique employs forward-DWT to decompose the noisy signals into various sub bands comprising high and low frequency wavelet coefficients. The high frequency coefficients are then modified using thresholding operation and denoised signals are obtained through inverse-DWT with the modified coefficients [18 - 20]. In use of such technique for BOTDA sensors, the decomposition of BGSs with higher level results more SNR enhancement, which in turn reduces the uncertainty in BFS extraction. However, such SNR enhancement is attained by thresholding high frequency wavelet coefficients of the measured BGSs [19, 20]. This thresholding operation can over-smooth the BGSs, particularly where the BFSs of the BGSs change sharply. Thus, higher enhancement of SNR achieved by decomposing measured BGSs with higher level also affects the spatial resolution of BOTDA sensors. Surprisingly, the consequence of decomposing measured BGSs with different levels used in wavelet denoising technique (WDT) on spatial resolution of sensors is not analyzed adequately in literature.

In this paper, the detailed performance of 2D DWT-based WDT is evaluated experimentally in denoising the noisy measured BGSs obtained from a BOTDA sensor along a 38. 2 km fiber. The CFM was then used to extract the distributions of BFS from the denoised BGSs. The advantages of using WDT-based CFM are analyzed for the BGSs acquired from BOTDA experiment using different frequency steps and different numbers of trace averaging. The effect of decomposing measured BGSs with different levels applied in WDT on spatial resolution of the sensor is also analyzed in this study.

2. BOTDA Experimental Setup

The experimental setup used in the laboratory in this study was a conventional [6, 7] BOTDA sensor as shown in the Fig. 1. The tunable laser used in the setup emits continuous wave (CW) at 1550 nm. Then the coupler splits the output of the laser and provides CW waves in the upper and lower branches. The polarization controllers (PC1 and PC2) in the two branches help to control the polarization states of CW waves. The pulse generator (PG) operates an electro-optic modulator (EOM1) for producing pump pulses by modulating the CW wave in the upper branch. Then an erbium-doped fiber amplifier (EDFA) is utilized to amplify the pulse power. The EDFA is followed by a band pass filter (BPF) whose function is to remove the amplified spontaneous emission (ASE) noise. Finally, the polarization scrambler (PS) in the upper branch is used to randomize the polarization states of the pump-pulses.

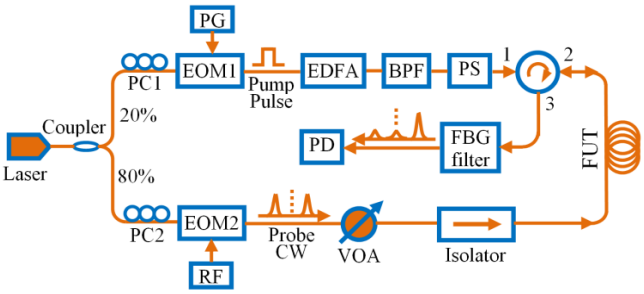

Fig. 1. Experimental setup of a conventional BOTDA sensor.

The radio-frequency (RF) signal generator in the lower branch controls another electro-optic modulator (EOM2). This EOM2 also modulates the CW wave but produces a double-side band suppressed-carrier probe signal in the lower branch. Then the variable optical attenuator (VOA) is employed to control the power of the CW probe signal and the isolator directs the probe signal in the forward direction through the FUT but prevents signal transmission from the backward direction.

Because of the interaction of counter-propagating pump and probe waves in the fiber, the probe signal is amplified. Then a fiber Bragg grating (FBG) filter allows only the desired low-frequency side band of the amplified probe signal to be detected by the photo detector (PD). The output of the PD is scanned subsequently at a particular pump-probe frequency difference around the local BFS of the FUT to obtain time-domain traces. These traces are then used to retrieve the BGSs along the FUT.

3. Operating Principle

3. 1 Discrete Wavelet Transform (DWT)

Wavelet transform is a powerful mathematical tool that is widely used for time-frequency analysis of signals [16 - 18]. The continuous wavelet transform (CWT) of a continuous-time signal $x(t)$ is expressed as

$$W_f(p,q) = \int_{-\infty}^{\infty} x(t)\psi_{p,q}(t)dt. \tag{1}$$

The continuous-time function $\psi_{p,q}(t)$ in Eq. (1) is defined by

$$\psi_{p,q}(t) = |p|^{-1/2}\,\psi\left(\frac{t-q}{p}\right) \tag{2}$$

where p and q, $p \neq 0$ and $(p,q) \in R$, are the dilation and translation parameters of the mother wavelet function $\psi(t)$ respectively. To formulate DWT from CWT, parameters p and q are discretized in dyadic form as $p=2^{-j}$ and $q=k2^{-j}$ where $(j, k) \in Z$. For such p and q, Eq. (2) can be used to express the discrete wavelet function as given by

$$\psi_{j,k}(t) = 2^{j/2}\psi(2^j t - k). \tag{3}$$

In Eq. (3), j is the dilation parameter which affects the scaling process and k is the translation parameter which affects the shifting process of the discrete wavelet function. With these two parameters j and k, a basis can be formed from the scaling and the wavelet functions given respectively by

$$\phi_{j,k}(t) = 2^{j/2}\phi(2^j t - k) \tag{4}$$

$$\psi_{j,k}(t) = 2^{j/2}\psi(2^j t - k). \tag{5}$$

Now, the functions given by Eqs. (4) and (5) can be applied to decompose any discrete-time signal $x(n)$ which yields

$$x(n) = \frac{1}{\sqrt{M}}\left[\sum_k A_\phi(j_0,k)\phi_{j_0,k}(n) + \sum_{j=j_0}^{\infty}\sum_k D_\psi(j,k)\psi_{j,k}(n)\right] \tag{6}$$

where $n = 0, 1, 2, \ldots, M\text{-}1$ and j_0 is an starting scale. Since $\phi_{j0,k}$ and $\psi_{j,k}$ are orthogonal to each other, the inner product can simply be used to obtain the approximation and detailed wavelet coefficients of $x(n)$ as given respectively by

$$A_\phi(j_0,k) = \frac{1}{\sqrt{M}}\sum_{n=0}^{M-1} x(n)\phi_{j_0,k}(n) \tag{7}$$

$$D_\psi(j,k) = \frac{1}{\sqrt{M}}\sum_{n=0}^{M-1} x(n)\psi_{j,k}(n). \tag{8}$$

It is worth to mention that the DWT can simply be realized via filter bank comprising low-pass and high-pass filters [17 - 18]. It is also easy to realize the 2D DWT from 1D DWT. For such realization, the filter bank structure of 1D DWT is successively applied along the rows and columns of a 2D discrete-time function [18 - 19].

3. 2 Wavelet Denoising Technique (WDT)

Wavelet denoising technique (WDT) makes use of wavelet transform for multi-resolution analysis of signals and images. The technique is easy to implement and

computationally efficient [18 - 22]. In this study, the BOTDA experimental setup shown in Fig. 1 is used for the acquisition of measured BGSs. The noisy measured BGSs are then denoised by employing 2D DWT-based multi-threshold WDT. The process of denoising BGSs using WDT is depicted in Fig. 2.

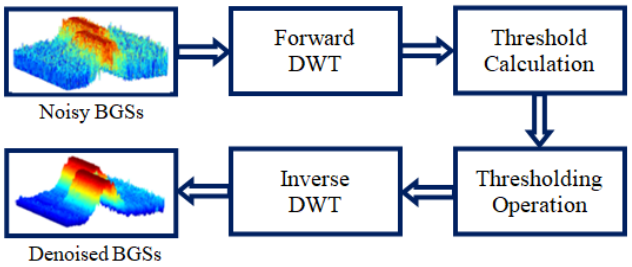

Fig. 2. Schematic diagram of WDT for denoising BGSs.

The process of WDT for denoising measured BGSs requires three steps. First, the measured BGSs are decomposed into sub bands by using forward-DWT. Then, level dependent thresholds are calculated and thresholding operation is performed to eliminate noise components. Finally, inverse-DWT is used on the thresholded sub bands to reconstruct the denoised BGSs. The first level decomposition (i. e. , L = 1) of noisy measured BGSs provides four sub bands, i. e. , approximation, horizontal detail, vertical detail and diagonal detail. The larger wavelet coefficients in the approximation sub band generally include main attributes of the BGSs. Other three detail sub bands mainly contain comparatively smaller wavelet coefficients and consist of noise attributes [18, 19]. For the multi-resolution analysis of noisy measured BGSs, a higher decomposition level (e. g. , L > 1) is adopted in WDT to obtain four new sub bands in each level by repeatedly decomposing the approximation sub band provided by the immediate previous level of BGSs decomposition.

Once the process of BGSs decomposition is over, Birgé-Massart strategy [18, 21] is used to calculate the thresholds for different detailed sub bands obtained after different levels of BGSs decomposition. Since the SNR of the noisy measured BGSs degrades gradually through the FUT, such BGSs along a small (e. g. , 1 km) span of the FUT are denoised using WDT so that the level dependent thresholds can be calculated precisely. Soft thresholding operation [21] is then performed only on the wavelet coefficients in detail sub bands, i. e., no thresholding operation on the wavelet coefficients in approximation sub band. Finally, the inverse-DWT is applied on the approximation sub band having unchanged wavelet coefficients and detail sub bands having modified wavelet coefficients to reconstruct the denoised BGSs. In the processes of decomposition and reconstruction of BGSs, the mother wavelet function *symlet*5 is used in this study.

3. 3 Curve Fitting Method (CFM)

After performing the process of BGSs denoising using WDT, BFS distributions along the FUT are extracted from the measured and denoised BGSs by using nonlinear least-square CFM. In CFM, Lorentzian profile [17, 23] given by

$$g(\upsilon) = \frac{g_B}{1+4\left[(\upsilon-\upsilon_B)/(\Delta\upsilon_B)\right]^2} \tag{9}$$

is employed as the model function, where g_B is the peak Brillouin gain, υ_B is the BFS and $\Delta\upsilon_B$ is the linewidth of the model function. The model function controlled by the vector $\mathbf{u} = [g_B, \nu_B, \Delta\nu_B]$ is fitted on to N sample points of a measured or denoised BGS so that the vector $\mathbf{u}$ is updated iteratively and the error function given by

$$E(\mathbf{u}) = \sum_{i=1}^{N}\left[g(\upsilon_i) - g(\upsilon_i, \mathbf{u})\right]^2 \tag{10}$$

is minimized. At the end of this fitting process, the updated υ_B of the model function in the vector $\mathbf{u}$ is supposed to be the BFS of the measured or denoised BGS. A short description and illustration of CFM can be found in Ref. [23].

4. Results and Discussion

In this study, the FUT used in the experimental setup of BOTDA sensor shown in Fig. 1 is 38. 2 km long. The last ~600 m portion of the FUT is unpacked from the fiber mandrel and wound manually with a diameter larger than that of the fiber mandrel. The unpacked ~600 m FUT is then put inside the oven. The temperature of the oven is set at 70 ^{o}C. Other portion of the FUT packed tightly on the fiber mandrel is kept outside the oven at room temperature of ~25 ^{o}C. The measured BGSs throughout the whole FUT of 38. 2 km long are acquired using the sampling interval of 0. 4 m and the pump pulse duration of 20 ns for obtaining 2 m spatial resolution of the sensor. The distribution of BGSs acquired using trace averaging of N_{av} = 100 and frequency step of $\Delta\upsilon$ = 1 MHz is shown in Fig. 3(a). The WDT is then used to denoise the noisy measured BGSs shown in Fig. 3(a). Such denoising process is repeated by adopting six different levels (i. e. , L = 1 to 6) of BGSs decomposition in WDT. For example, the distributions of denoised BGSs obtained by using WDT with L = 2, 4, and 6 are shown in Figs. 3(b)-(d), respectively.

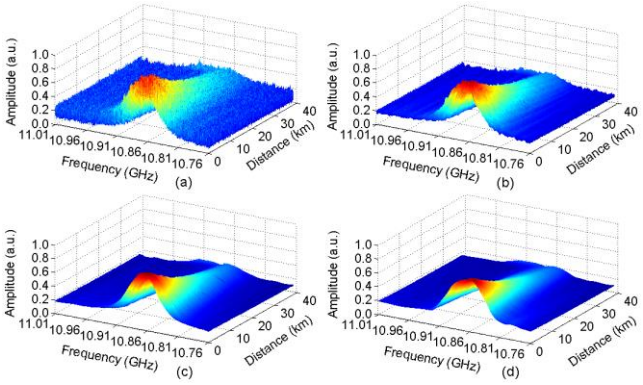

Fig. 3. Distributions of (a) the noisy measured BGSs, and the denoised BGSs along the 38. 2 km long FUT obtained by using WDT with different levels of BGSs decomposition of (b) L = 2, (c) L = 4 and (d) L = 6.

It was observed from the distributions of measured and denoised BGSs in the Fig. 3 that 2D DWT-based WDT can reduce noise significantly from the noisy measured BGSs. It is remarkable in the Fig. 3 that WDT with higher level of BGSs decomposition also provides lower level of noise in the denoised BGSs.

Next, curve fitting method (CFM) was employed for extracting BFS distributions from the noisy measured and denoised BGSs throughout the whole span of 38. 2 km FUT. The distribution of BFS along the FUT for the noisy measured BGSs shown in the Fig. 3(a) without applying WDT is plotted in the Fig. 4(a). The distributions of BFS from the denoised BGSs throughout the whole span of the FUT are also extracted separately after applying WDT with L = 1 to 6, i. e. , six different levels of BGSs decomposition. For instance, the distributions of BFS for the denoised BGSs along the FUT shown in Figs. 3(b)-(d) obtained after employing WDT with L = 2, 4 and 6 are plotted in Figs. 4(b)-(d), respectively.

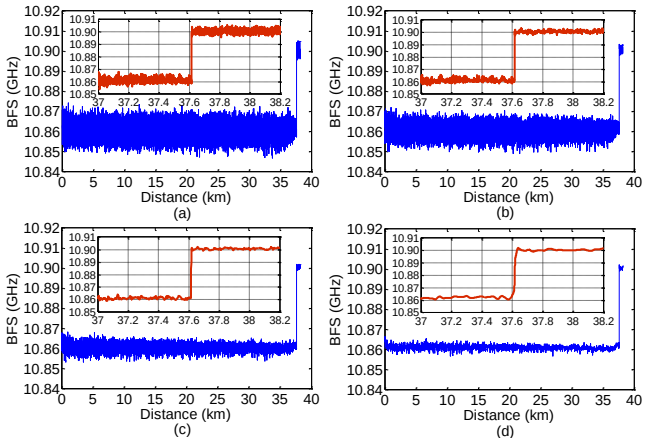

Fig. 4. BFS distributions along the 38. 2 km long FUT for (a) the noisy measured BGSs, and the denoised BGSs obtained by using WDT with different levels of BGSs decomposition of (b) L = 2, (c) L = 4 and (d) L = 6. Inset: BFS distributions along the last 1200 m portion of the FUT.

It is clear from the Fig. 4 that the BFSs along the FUT in the Fig. 4(a) extracted from the noisy measured BGSs without utilizing WDT fluctuate largely as compared to that extracted from the denoised BGSs obtained after utilizing WDT in Figs. 4(b)-(d). In addition, such fluctuations in Figs. 4(b)-(d) decrease greatly when WDT adopts higher level of BGSs decomposition and become significantly smaller for L = 6, the highest level of BGSs decomposition adopted in this study. Thus, the uncertainty in BFS extraction using CFM decreases largely when WDT with higher decomposition level is adopted to denoise the noisy measured BGS. It is noteworthy that the relatively large fluctuations in the extracted BFS distributions in Fig. 4, especially at the beginning of the FUT are originated owing to the existence of irregular strain along the FUT packed tightly on the fiber mandrel where, the diameter of the packed fiber at the beginning is relatively small (i. e. , more strain) than that at the end of the FUT.

The distributions of BGSs in Fig. 3 and their BFS distributions in Fig. 4 indicate that WDT can enhance the measurement SNR significantly and thus, the uncertainty in BFS extraction reduces greatly. To assess the performance of WDT quantitatively, the SNRs of the noisy measured and denoised BGSs and the corresponding uncertainties in BFS extraction are calculated. For this calculation, the last 500 m portion (worst SNR and uncertainty) of the FUT starting from 37. 7 km to 38. 2 km heated at 70^{o} C inside the oven is considered. The SNR for a BGS is calculated to be the ratio of maximum gain of its fitted curve and the standard deviation of its residuals from the fitted curve [7,16]. The calculated SNRs for all the BGSs within the selected 500 m portion the FUT are then averaged to estimate the SNR for the portion. To determine the uncertainty in BFS extraction, the standard deviations of the extracted BFSs along the portions of few meters (e. g. , 25 m) within the last 500 m FUT [6] are computed. The uncertainty is then calculated by averaging the nearly equal standard deviations for all portions within the last 500 m fiber. The SNRs and uncertainties for the noisy measured BGSs without using WDT (i. e. , L = 0) and denoised BGSs obtained using WDT with L = 1 to 6 are shown in Fig. 5.

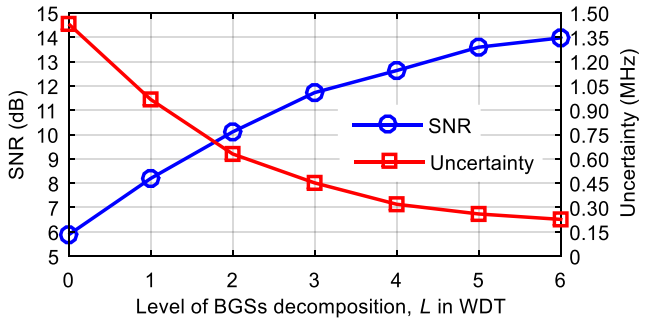

Fig. 5. Variation of SNR of BGSs and uncertainty in BFS extraction for the decomposition of BGSs with different levels, L in WDT.

It is evident from Fig. 5 that the use of WDT helps to obtain several times improvement of the measurement SNR, which in turn reduces the uncertainty in BFS extraction significantly. For example, the SNR in Fig. 5 calculated for the noisy measured BGSs without applying WDT (i. e. , L = 0) is ~5. 88 dB which is improved by an amount of ~4. 23 dB, ~6. 75 dB and ~8. 09 dB (i. e. , by the factors of ~2. 65, ~4. 73 and ~6. 45 respectively) for adopting L = 2, 4 and 6 in WDT. For such improvement of SNR, the uncertainty in BFS extraction is reduced from ~1. 43 MHz to ~0. 63 MHz, ~0. 32 MHz and ~0. 23 MHz (i. e. , by the factors of ~2. 27, ~4. 47 and ~6. 32 respectively) for applying WDT with L = 2, 4 and 6.

The results shown in Fig. 5 clearly reveal that the decomposition of BGSs in WDT adopting higher level (L) expedites the enhancement of SNR which, in turn reduces the uncertainty in BFS extraction. However, the use of higher L in WDT can greatly instigate the loss of the high frequency wavelet components to make the BGSs over-smoothed, particularly where the BFSs of the BGSs change sharply [19, 20]. As a result, the spatial resolution of the

sensors can also be affected due to the adaptation of higher L in WDT. To study this effect, the distributions of BFS along the portion of the FUT where the BFSs of the BGSs change sharply from ~25 °C to 70 °C are extracted by adopting different L in WDT. Such distributions of BFS are shown in Fig. 6. The results show that the lower level decomposition (e. g. , L = 1 and 2) of BGSs in WDT can maintain the actual spatial resolution of the sensor. However, it is also needed to sacrifice the spatial resolution of the BOTDA sensor if the decomposition level adopted in WDT is greater than L = 2.

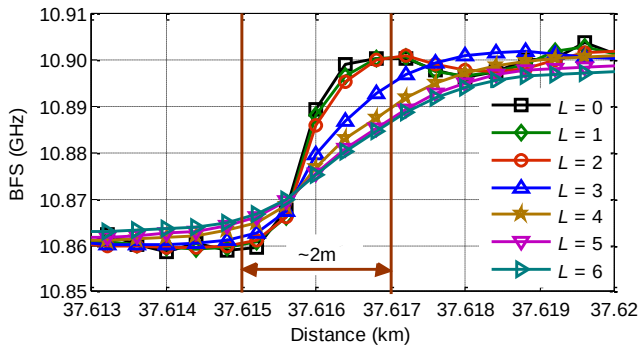

Fig. 6. Variation of spatial resolution of the sensor for the decomposition of BGSs with different levels, L in WDT.

The BFS distributions shown in Fig. 6 signify that the highest decomposition level of L = 2 can safely be employed in WDT for denoising the noisy measured BGSs so as to maintain the 2 m spatial resolution of the sensor adopted in this study. The decomposition of BGSs using such level (i. e. , L = 2) in WDT can reduce the uncertainty in BFS extraction from ~1. 43 MHz to ~0. 63 MHz (i. e. , ~56%) as can be observed from Fig. 5. However, it is also noticed in Fig. 5 that the uncertainty in BFS extraction can be reduced further from ~1. 43 MHz to ~0. 23 MHz (i. e. , ~84%) for L = 6. In such case, the BFS distributions in Fig. 6 indicate that the actual spatial resolution (i. e. , 2 m) of the sensor cannot be guaranteed.

Now, the WDT-based CFM is applied to the measured BGSs acquired at different frequency steps ($\Delta\upsilon$) for evaluating the performance of this method. For this, the noisy measured BGSs at ten different frequency steps of $\Delta\upsilon$ = 1 to 10 MHz are obtained by down-sampling the noisy measured BGSs shown in Fig. 3(a) obtained at $\Delta\upsilon$ = 1 MHz and N_{av} = 100. Such BGSs are first denoised separately by applying WDT with different levels of BGSs decomposition and then the CFM is employed to extract the BFS distributions from the measured and denoised BGSs for each $\Delta\upsilon$ and L. The uncertainties in BFS extraction within the last 500 m FUT for different $\Delta\upsilon$ and L are shown in Fig. 7.

It is noticed from the Fig. 7 that the uncertainty in BFS extraction for applying CFM with WDT is considerably smaller as compared to that without applying WDT at each of the ten different frequency steps and the uncertainty increases gradually for the BGSs acquired at larger frequency step. For instance, the uncertainty in BFS extraction without employing WDT to the measured BGSs acquired at $\Delta\upsilon$ = 5 MHz in Fig. 7 is 3. 32 MHz, which decreases to 1. 41 MHz for employing WDT with L = 2. Thus, the denoising of BGSs obtained at $\Delta\upsilon$ = 5 MHz employing WDT with L = 2 can improve the uncertainty in BFS extraction by a factor of ~2. 39 (i. e. , ~58%). It is also noticed from Fig. 7 that the uncertainty in BFS extraction for employing WDT with L = 2 to the noisy measured BGSs obtained at $\Delta\upsilon$ = 5 MHz is 1. 41 MHz, which is comparable to the uncertainty of 1. 43 MHz for the noisy measured BGSs acquired at $\Delta\upsilon$ = 1 MHz without employing WDT. However, such arrangement with WDT permits the use of 5 times larger frequency step to acquire BGSs from the BOTDA experiment and thus, the acquisition time can greatly be reduced by ~80%.

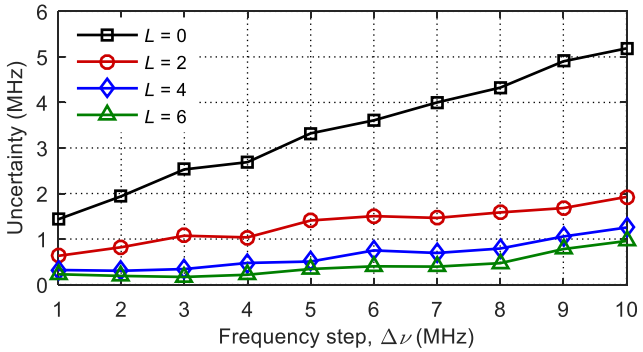

Fig. 7. Variation of uncertainty in BFS extraction with frequency step used to obtain the BGSs at trace averaging number of N_{av} = 100.

Next, the WDT-based CFM is applied to the noisy measured BGSs acquired using ten different numbers of trace averaging starting from N_{av} = 100 to 1000 to evaluate the performance of the method. For this evaluation, the measured BGSs of each of the ten different N_{av} obtained at $\Delta\upsilon$ = 1 MHz are denoised individually by employing WDT with different levels of BGSs decomposition. Then, the CFM is employed for extracting the BFS distributions from the measured and denoised BGSs for each N_{av} and L. The uncertainties in BFS extraction given by CFM with WDT for adopting different L and that without employing WDT are then computed for the last 500 m portion of the FUT. The variations of uncertainty with N_{av} for different level of BGSs decomposition in WDT are shown in Fig. 8.

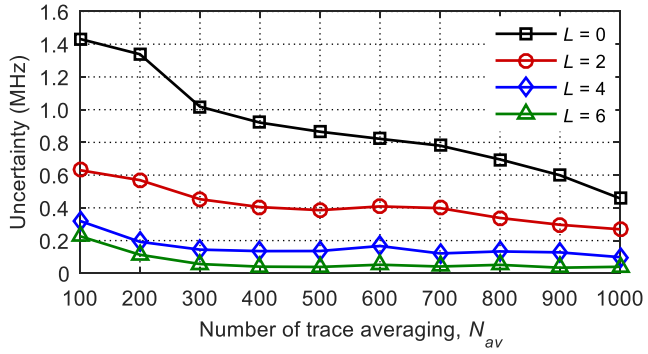

Fig. 8. Variation of uncertainty in BFS extraction with number of trace averaging used to obtain the BGSs at frequency step of $\Delta\upsilon$ = 1 MHz.

The results in the Fig. 8 demonstrate that the uncertainty in BFS extraction decreases gradually when large number of trace averaging was adopted to improve the SNR of the measured BGSs [6, 7]. It was evident from Fig. 8 that the CFM with WDT provide much lower eruncertainty in BFS extraction at each level of BGSs decomposition as compared to that without applying WDT (i. e. , L = 0). The results in Fig. 8 also confirm that the uncertainty in BFS extraction decreases significantly when higher level of BGSs decomposition is adopted in WDT. However, the BFS distributions in Fig. 6 confirm that the BGSs decomposition level up to L = 2 could only ensure the preservation of spatial resolution. For using WDT with L = 2, the uncertainty in extracting BFS from the noisy measured BGSs obtained using N_{av} = 100 is ~0. 63 MHz, which is comparable to that of ~0. 70 MHz using N_{av} = 800 without employing WDT. Consequently, WDT with L = 2 can provide comparable performance by adopting 87. 50% less trace averaging, which help to significantly reduce the time required to acquire BGSs from the BOTDA experiment.

Finally, the computational complexity and runtime of WDT-based CFM are analyzed and evaluated quantitatively in extracting BFS distributions from the noisy measured BGSs. The computational complexity of 1D DWT is on the order of $O(L)$ if L is the number of sample points in a 1D signal [24]. In 2D DWT, the 1D DWT is alternatively applied first on the each row and then on the each column of the noisy measured BGSs. The computational complexity of 2D forward-DWT used to obtain wavelet coefficients by decomposing M BGSs each having N sample points into different sub bands thus becomes on the order of $O(MN)$. Since the reconstruction of the denoised BGSs from the thresholded wavelet coefficients using inverse-DWT also requires same computational effort, the computational complexity of WDT becomes on the order of $O(2MN)$ for denoising M BGSs [25], which is equivalent to the computational complexity of $O(2N)$ for each BGS. Each of the denoised BGSs obtained with WDT is then fitted using nonlinear least-square CFM whose computational complexity is on the order of $O(\eta N^2)$ where η denotes the number of iterations taken by the CFM to update the model parameters [7]. As a consequence, the WDT-based CFM suffers from the computational complexity that is on the order of $O(2N+\eta N^2)$ in which the major part is introduced by the CFM. In order to compare the signal processing speed of CFM with applying WDT and that without applying WDT quantitatively, the runtimes required to extract BFS distributions are computed for the measured BGSs obtained with N_{av} = 100 and ten different frequency steps $\Delta\upsilon$ as well as that with $\Delta\upsilon$ = 1 MHz and ten different trace averaging numbers N_{av}. The relative runtime is then calculated by dividing each of these runtimes by the runtime required for the noisy measured BGSs acquired with $\Delta\upsilon$ = 1 MHz and N_{av} = 100. The variation of relative runtime with ten different frequency steps $\Delta\upsilon$ for N_{av} = 100 and that with ten different trace averaging numbers N_{av} for $\Delta\upsilon$ = 1 MHz are plotted in Fig. 9 and Fig. 10 respectively.

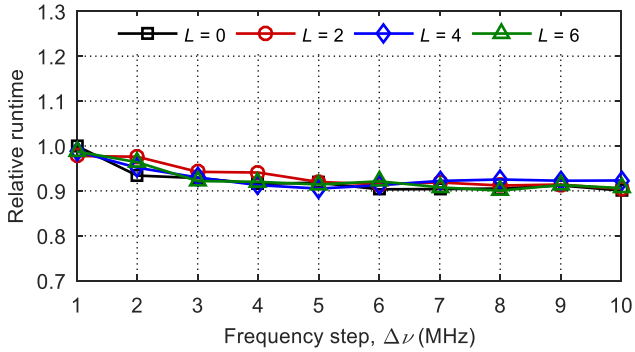

Fig. 9. Variation of relative runtime in BFS extraction with frequency step used to obtain the BGSs using trace averaging number of N_{av}= 100.

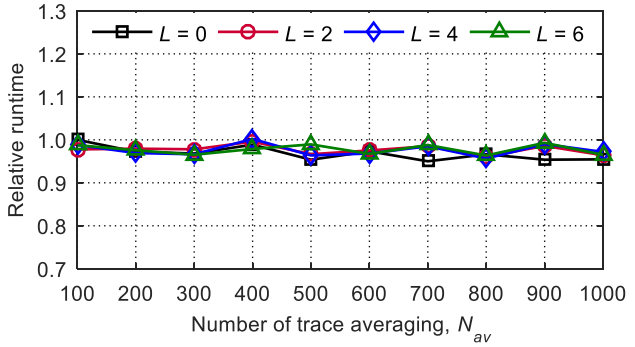

Fig. 10. Variation of relative runtime in BFS extraction with number of trace averaging used to obtain the BGSs at frequency step of $\Delta\upsilon$ = 1 MHz.

It is clear from Fig. 9 and Fig. 10 that the relative runtimes of using CFM with WDT for different levels (e. g. , L = 2, 4 and 6) of BGSs decomposition and that using CFM without WDT (i. e. , L = 0) are almost the same. The results validate that the denoising of noisy measured BGSs using WDT does not include significant processing time to the WDT-based CFM. It is noticed from Fig. 9 that the relative runtimes in extracting BFS from the BGSs obtained at smaller $\Delta\upsilon$ are relatively larger than that at higher $\Delta\upsilon$. This is due to the fact that the number of sample points (N) on each BGS obtained using a smaller $\Delta\upsilon$ is also larger. The results in Fig. 10 for $\Delta\upsilon$ = 1 MHz (i. e. , same N) also shows a very little decrease in relative runtime for the BGSs obtained using larger N_{av}. This is due to the fact that SNRs of BGSs obtained using larger N_{av} is also higher. As a result, the CFM needs relatively small number of iterations (i. e. , smaller η) to fit the measured BGSs acquired with larger N_{av} as compared to that obtained with smaller N_{av}. The results in Fig. 9 and Fig. 10 also confirm that the relative run times in BFS extraction using WDT-based CFM with different levels (L) of BGSs decomposition do not change significantly. This is because a larger L in WDT also provides denoised BGSs with larger SNR. As a result, the CFM also takes relatively small number of iterations (i. e. , smaller η) to fit the denoised BGSs.

5. Conclusions

In this paper, the experimental analysis of 2D DWT-based WDT is demonstrated for denoising BGSs acquired from

BOTDA sensors. The CFM is then applied to the denoised BGSs for the accurate extraction of BFS distributions along the FUT. The performance of WDT-based CFM is evaluated for the noisy measured BGSs acquired from BOTDA experiment with different frequency steps and different numbers of trace averaging. The effects of decomposing BGSs with different levels adopted in WDT are also analyzed explicitly and the results suggest that decomposition level up to 2 can be safely adopted to improve the uncertainty in BFS extraction up to ~56% while maintaining the actual spatial resolution of the sensor, which is 2 m in this study. However, the decomposition of BGSs adopting lager level in WDT allows the further improvement of uncertainty in BFS extraction with a little sacrifice of spatial resolution. Moreover, under a given uncertainty and spatial resolution, BFS extraction using WDT-based CFM can effectively adopt either 5 times larger frequency step or ~87. 50% less trace averaging to significantly reduce the acquisition time of BOTDA-measured BGSs. In addition, WDT is a computationally efficient algorithm which does not include significant signal processing time to CFM. Therefore, WDT-based CFM can be an attractive alternative for the accurate and faster extraction of BFS distributions from the noisy measured BGSs acquired from BOTDA sensors.

Acknowledgement

The author thankfully acknowledges the support of the PolyU Photonics Research Center, The Hong Kong Polytechnic University for providing the facility of the laboratory experiment.

References

1. C. A. Galindez-Jamioy, and J. M. Lopez-Higuera, 2102, "Brillouin Distributed Fiber Sensors: An Overview and Applications," *J. of Sensors* 2012, Article ID 204121, pp 1-17.
2. M. A. Soto, X. Angulo-Vinuesa, S. Martin-Lopez, S. Chin, J. D. Ania-Casta˜non, P. Corredera, E. Rochat, M. Gonzalez-Herraez, and L. Th´evenaz, 2014, "Extending the real remoteness of long-range Brillouin optical time-domain fiber analyzers," *J. Lightwave Technol.* 32(1), pp 152–162.
3. B. Wang, L. Wang, N. Guo, Z. Zhao, C. Yu, and C. Lu, 2019, "Deep neural networks assisted BOTDA for simultaneous temperature and strain measurement with enhanced accuracy,"*Opt. Express*, 27(3), pp 2530-2543.
4. Y. Dong, L. Chen, and X. Bao, 2011, "Time-division multiplexing-based BOTDA over 100 km sensing length," *Opt. Lett.* 36(2), pp 277-279.
5. A. Kobyakov, M. Sauer, and D. Chowdhury, 2010, "Stimulated Brillouin scattering in optical fibers," *Adv. Opt. and Photon.* 2(1), pp 1-59.
6. M. A. Soto, and L. Thévenaz, 2013, "Modeling and evaluating the performance of Brillouin distributed optical fiber sensors," *Opt. Express*, 21(25), pp 31347-31366.
7. A. K. Azad, F. N. Khan, W. H. Alarashi, N. Guo, A. P. T. Lau and C. Lu, 2017, "Temperature extraction in Brillouin optical time-domain analysis sensors using principal component analysis based pattern recognition," *Opt. Express*, 25(14), pp 16534-16549.
8. X. Jia, and Y. Rao, L. Chang, C. Zhang and Z. Ran, 2010, "Enhanced sensing performance in long distance Brillouin optical time-domain analyzer based on Raman amplification: Theoretical and experimental investigation," *J. Lightwave Technol.* 28(11), pp 1624–1630.
9. M. A. Soto, G. Bolognini, and F. D. Pasquale, 2011, "Optimization of long-range BOTDA sensors with high resolution using first-order bidirectional Raman amplification," *Opt. Express*, 19(5), pp 4444-4457.
10. X. Angulo-Vinuesa, S. Martin-Lopez, P. Corredera, and M. Gonz´alez-Herr´aez, 2012, "Raman-assisted Brillouin optical time-domain analysis with sub-meter resolution over 100 km," *Opt. Express*, 20(11), pp 12147-12154.
11. M. A. Soto, G. Bolognini, F. Di Pasquale, and L. Thévenaz, 2010, "Long-range optical time-domain analysis employing pulse coding techniques," *Meas. Sci. Technol.* 11(9), pp 1–7.
12. Y. Mao, N. Guo, K. L. Yu, H. Y. Tam and C. Lu, 2012, "1-cm-Spatial-Resolution Brillouin Optical Time-Domain Analysis Based on Bright Pulse Brillouin Gain and Complementary Code,"*IEEE Photonics. J.* 4(6), pp 2242-2248.
13. H. Iribas, A. Loayssa, F. Sauser, M. Llera, and S. L. Floch, 2017, "Cyclic coding for Brillouin Optical Time-Domain Analyzer using probe dithering," *Opt. Express*, 25(8), pp 8787-8800.
14. M. A. Soto, M. Taki, G. Bolognini, and F. D. Pasquale, 2012, "Simplex-coded BOTDA sensors over 120 km SMF with 1-m spatial resolution assisted by optimized bidirectional Raman amplification," EEE *Photon. Tech. Lett.* 24(20), pp 1823-1826.
15. H. Wu, L. Wang, Z. Zhao, N. Guo, C. Shu, and C. Lu, 2018, "Brillouin optical time domain analyzer sensors assisted by advanced image denoising techniques. ," *Opt. Express*, 26(5), pp 5126-5139.
16. M. A. Soto, J. A. Ramírez, and L. Thévenaz, 2016, "Intensifying the response of distributed optical fibre sensors using 2D and 3D image restoration," *Nat. Commun.* 7:10870.
17. M. A. Farahani, M. T. V. Wylie, E. Castillo-Guerra, and F. G. Colpitts, 2012, "Reduction in thenumber of averages required in BOTDA sensors using wavelet denoisingtechniques," *J. Lightwave Technol.* 30(8), pp 1134–1142.
18. S. Sidhik, 2015, "Comparative study of Birge–Massart strategy and unimodal thresholding for image compression using wavelet transform," *Optik- Int. J. for Light and Elect. Optics*, 126(24), pp 5952-5955.
19. A. SOVIĆ, and D. SERŠIĆ, 2012,"Signal decomposition methods for reducing drawbacks of DWT,"*Eng. Rev.* 32(2), pp 70–77.
20. Y. P. Chaudhari, and P. M. Mahajan, 2017, "Image denoising of various images using wavelet transform and thresholding techniques," *Int. Research. J. Engg. Technol.* 4(2), pp 517-523.
21. K. Daqrouq, I. N. Abu-Isbeih, O. Daoud, and E. Khalaf, 2010, "An investigation of speech enhancement using wavelet filtering method,"*Int. J. speech Technol.* 13(2), pp 101-115.
22. Z. Qin, L. Chen, and X. Bao, 2012, "Continuous wavelet transform fornon-stationary vibration detection with phase-OTDR," *Opt. Express*, 20(18), pp 20459–20465.

23. A. K. Azad, L. Wang, N. Guo, H. Y. Tam and C. Lu, 2016, "Signal processing using artificial neural network for BOTDA sensor system," *Opt. Express*, 24(6), pp 6769-6782.

24. S. Attallah,2000,"The wavelet transform-domain LMS algorithm: a more practical approach," *IEEE Trans. On Circuits Systems-II: analog & digital signal process.* , 47(3), pp 209-213.

25. A. Shahbahrami, 2012, "Algorithms and architectures for 2D discrete wavelet transform," *J. supercomput*, 62, pp 1045-1064.